JPE 16-3-25

http://dx.doi.org/10.6113/JPE.2016.16.3.1076
ISSN(Print): 1598-2092 / ISSN(Online): 2093-4718

A Novel Method to Suppress Mid-Frequency Vibrations with a High Speed-Loop Gain for PMSM Control

Qiong Li†, Qiang Xu*, and Shenghua Huang*

†,*Department of Electronic Engineering, Huazhong University of Technology and Science, Wuhan, China

Abstract

PI controllers are one of the most widely used controllers in industrial control systems due to their simple algorithms and stability. The parameters K_p and K_i determine the performance of the system response. The response is expected to improve by increasing the gain of the PI controller. However, too large a gain will accelerate the speed response and cause vibrations, which is not what is expected. This paper proposes a way to suppress vibrations by detecting the vibration frequency and extracting the vibration signal as a compensation to the speed feedback. Additionally, in order to improve its disturbance rejection ability, a low-order disturbance observer is proposed. This paper also explains the operation principle of the proposed method by analyzing the transfer function and it describes the design of the controller parameters in detail. Simulation and experimental results are provided to verify the merits of the proposed method. These results also show the good performance of the proposed method. It has a rapid response and suppresses vibrations.

Key words: AC motor drives, Robust control, Speed control, Vibration control

I. INTRODUCTION

AC servo systems are widely used in industrial applications due to their simple structure and easy maintenance. Common applications include CNC engraving machines and milling machine. Improving the performance of PMSM control is significant for many of its applications. A PI controller is one of the most advanced controllers. The control algorithm is simple, and the parameters are few and easy to tune. These advantages make PI controllers the most commonly used in industrial applications. It is reported that more than 90% of control systems use a PI control algorithm [1]. The parameters Kp and Ki determine the performance of the controller. Generally, these parameters are designed to make the response as quick as possible without reducing its stability. Increasing Kp can accelerate the speed response. However, a Kp that is too large can bring vibrations and make the system unstable. In order to ensure stable operation conditions and to reduce oscillations, many methods have been presented by scholars.

In [2], Chengbin Ma designed and analyzed the performance of a number of PID structures including the integral-proportional (IP), the modified IP (m-IP), and the modified integral-proportional-derivative (m-IPD). It was shown that these IP and m-IPD controllers can effectively suppress vibrations. However, these structures should be changed according to the inertia ration which decreases the generality of their application. In [3], [4], a fractional order controller was adopted to solve the problem of the contradiction between the stability margin loss and the strength of the vibration suppression. However, the design of the fractional order controller is difficult and the realization is somewhat problematic. Wen Li proposed a single neuron-based PI fuzzy controller and a fractional-order disturbance observer for vibration suppression [5]. The PI fuzzy controller was used to obtain a desired steady-state precision and the observer was applied to generate a compensation signal. The results showed that this improved the speed loop control. However, while the robustness of the disturbance observer local loop to parameters variations was discussed, that of closed loop has not been considered. Jul-Ki Seok combined P and PI controllers to achieve speed control [6]. However, the controller switching

Manuscript received Sep. 18, 2015; accepted Dec. 29, 2015
Recommended for publication by Associate Editor Bon-Gwan Gu.
†Corresponding Author: powerdsp@hust.edu.cn
Tel: +86-130, Fax: +86-027-8654662, Huazhong Univ. of Sci. & Tech
*Dept. of Electronic Eng., Huazhong University of Technology and Science, China

point was set manually, and the adjustable drive performance was seriously dependent on the approximate point. Jong-Sun Ko presented a neural load torque compensation method to obtain better precision control [13]. Wan-Cheng Wang proposed a systematic wavelet control algorithm to obtain faster command responses and better load disturbance responses for the speed-loop control system or the position control system [14]. Experimental results verified the correctness of the proposed method. However, the experiments were only tested for a micro PMSM. Z. Zhiqiang built a relationship between the PID parameters and the oscillation characteristics of the closed loop response, and proposed a PID parameter tuning strategy according to the oscillation characteristics [17]. However, this study only provided simulation results, and experiments should be conducted. Hanifzadegan proposed a parallel structure of a feedback controller to suppress vibrations during operation [18]. One controller aims at improving the tracking performance and the other controller is used to reduce the peak amplitude at the resonance frequency. However, the performances of the controllers contradict each other.

In this paper, a strategy to improve the speed response while maintaining stability is presented without changing the classical PI structure. The method is based on detecting the speed vibration signal. The vibration frequency can be calculated by analyzing the speed error with a FFT. Then the speed vibration signal is extracted as compensation for speed feedback. Additionally, a low-order Luenberger observer is used to improve the anti-disturbance ability. The effectiveness of the proposed control system is verified by simulation and experimental results.

II. PMSM Model and Problem Formulation

A. PMSM Control System Modeling

The mechanical and electrical subsystem of a PMSM can be denoted as follows:

$$\frac{d\theta}{dt} = \omega \tag{1a}$$

$$\frac{d\omega}{dt} = \frac{1}{J_m}(T_m - T_L - B\omega) \tag{1b}$$

$$\frac{di_d}{dt} = \frac{1}{L_d}(u_d + \omega L_q i_q - Ri_d) \tag{1c}$$

$$\frac{di_q}{dt} = \frac{1}{L_q}(u_q - \omega L_d i_d - Ri_q - \omega\psi_m) \tag{1d}$$

Where eq. (1a) and eq. (1b) describe the mechanical subsystem, and (1c) and (1d) show the electrical subsystem equations. θ, ω are the motor angle and speed; i_d, i_q are the d-q axes stator currents; u_d, u_q are the d-q axes stator voltages; R is the stator resistance; L_d, L_q are the d-q axes stator inductances; J_m is the moment of inertia; B is the damping factor; ψ_m is the flux linkage; T_L is the load torque; and T_m is the electrical torque.

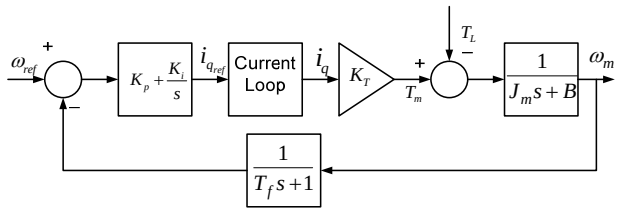

Fig. 1. The classical speed control structure.

B. Speed PI Control Module

Fig. 1 describes the PI control structure under a speed loop. Where ω_{ref} is the speed command, ω_m is the rotor speed, i_{qref} is the current command, i_q is the practical current, T_f is the low-pass filter time constant of the speed feedback, and K_T is the torque coefficient.

The target of the speed PI control module is to generate i_{qref}.

$$i_{qref} = K_p(\omega_{ref} - \omega_{fed}) + K_i\int_0^t(\omega_{ref} - \omega_{fed})dt \tag{2}$$

The transfer functions need to be analyzed: $\omega_m(s)/\omega_{ref}(s)$, $\omega_m(s)/T_L(s)$. First, the current close-loop transfer function should be obtained. Generally, the current transfer function is corrected as a traditional second-order system. Since the bandwidth of the speed loop is far below the current-loop bandwidth, it is possible to neglect the high-order items in the transfer function without influencing the analysis of the whole system. Thus, it is possible to rewrite the current close loop as eq. (3).

$$G_c(s) = \frac{1}{2T_c s + 1} \tag{3}$$

$$T_c = T_{cf} + T_{sf} \tag{4}$$

Where T_{cf} is the current feedback filter time constant, and T_{sf} is the inverter switching period. Then it is possible to derive the transfer function $\omega_m(s)/\omega_{ref}(s)$, $\omega_m(s)/T_L(s)$ as follows:

$$G = (K_p + \frac{K_i}{s})\frac{K_T}{2T_c s + 1}\frac{1}{J_m s + B} \tag{5}$$

$$H = \frac{1}{T_f s + 1} \tag{6}$$

$$H_{RR}(s) = \frac{\omega_m(s)}{\omega_{ref}(s)} = \frac{G}{1 + GH} \tag{7}$$

$$G' = \frac{1}{J_m s + B} \tag{8}$$

$$H' = \frac{1}{T_f s + 1}(K_p + \frac{K_i}{s})\frac{K_T}{2T_{cf} s + 1} \tag{9}$$

$$H_{RL}(s)=\frac{\omega_m(s)}{T_L(s)}=-\frac{G'}{1+G'H'} \quad (10)$$

From eq. (7) and eq. (10), it can be seen that the speed response depends on how much of ω_{ref} can be passed by $H_{RR}(s)$. It can also be seen that the system robustness depends on how much of T_L can be rejected by $H_{RL}(s)$. Here the motor parameters in Table I are used to see the influence of different K_p values on the performance of the control system.

Generally, the speed loop is designed to be a traditional II-system. Therefore, according to the design specifications of the traditional II-system, K_p and K_i can be calculated [23]. The first step is the elimination of $H_{RR}(s)$ and $H_{RL}(s)$ by the motor parameters and controller parameters. Then it is possible to obtain the bode diagrams of $H_{RR}(s)$ and $H_{RL}(s)$ under different K_p values as shown in Fig. 2(a) and Fig. 2(b). The figures illustrate that the bode diagram of $H_{RR}(s)$ peaks when K_p is big enough. According to the characteristics of a second-order system, the resonance peak leads to speed vibrations. A larger K_p helps improve the disturbance rejection since the magnitude of disturbance frequency response is lower. However, it also peaks at the vibration frequency. In conclusion, increasing the gain of the speed PI controller can speed up the rapidity of the speed response. However, it may bring vibrations and weaken stability.

C. The Relationship between the Vibration Frequency and Kp

Assuming T_f=0, B=0. Therefore, $H_{RR}(s)$ can be denoted by the following:

$$\frac{K_T K_p s+K_i}{J_m s^2+K_T K_p s+K_i}=\frac{K_T K_p s+K_i}{(\frac{s}{\omega_n})^2+2\xi\frac{s}{\omega_n}+1}$$

where $\omega_n=\sqrt{K_i/J_m}$ is the natural frequency and ξ is the damping coefficient. According to the second-order system frequency response, the resonance frequency is defined as $\omega_{vib}=\sqrt{1-2\xi^2}\omega_n$. Therefore, so the resonance frequency of eq. (7) is $\omega_{vib}=\sqrt{K_i K_T/J_m-K_T K_p^2/2J_m K_i}$. Since $K_i=K_p/\tau$, where τ is the time constant, it can be rewritten as $\omega_{vib}=\sqrt{K_p K_T/(\tau J_m)-\tau K_T K_p/(2J_m)}$. It is well known that τ is a very small constant, and that ω_{vib} is close to $\sqrt{K_p K_T/(\tau J_m)}$.

III. Proposed Method for the Control Module

To reduce the speed vibration in the control system, a control strategy is proposed, as shown in Fig. 3, where k and k_{vib} are the control parameters of the disturbance torque observer and speed vibration observer, respectively, k_{lf} is the cut-off frequency of the low-pass filter, LF represents the low-pass

TABLE I
The Simulation Parameters

Para.	Values	Unit
J_m	8e-3	Kg.m2
Rs	2.87	Ω
L_q	8.5e-3	H
K_T	1	Nms
T_{sf}	0.002	s
T_{cf}	40	μs
T_f	2	ms

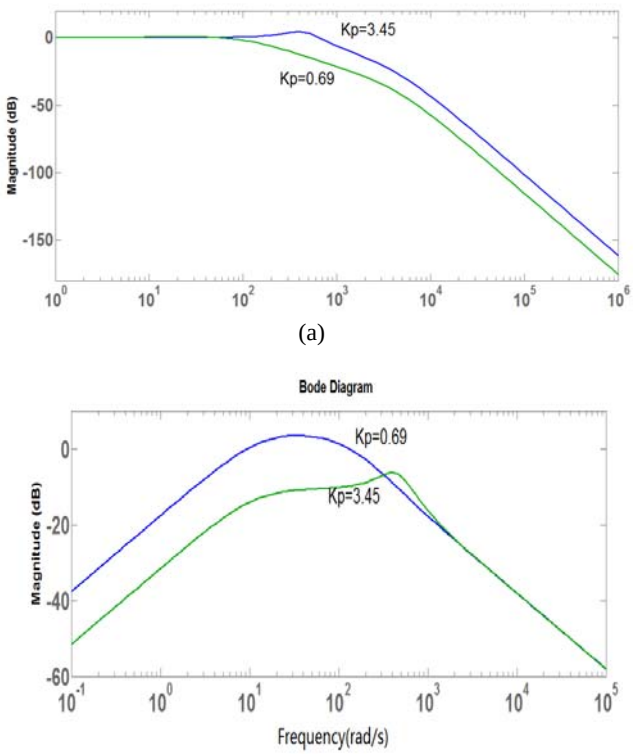

(a)

(b)

Fig. 2. (a) The bode diagrams of $H_{RR}(s)$. (b) The bode diagrams of $H_{RL}(s)$.

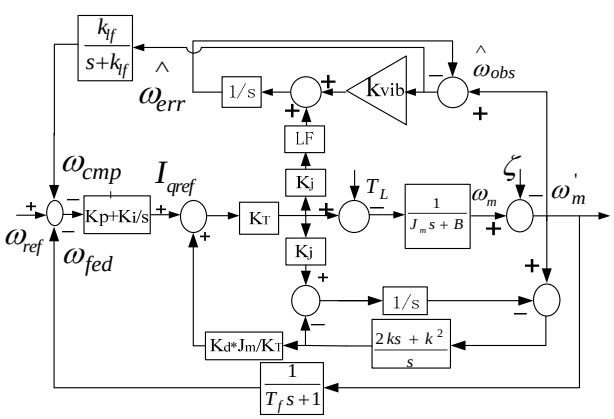

Fig. 3. The proposed method's structure.

filter, k_j is the reciprocal value of the inertia, and ζ is the measurement noise. Through the analysis of how K_p affects the performance of the control system in section II.B, it can be seen that the key to suppressing the oscillation induced by a large K_p is to reduce the magnitude at the resonance frequency. The following sections will describe how to implement the method to achieve the target.

A. Disturbance Torque Observer

A disturbance observer can help improve the robustness of the control system. Here, a Luenberger observer is used to estimate the disturbance torque. Fig. 4 shows the structure of the proposed disturbance observer. Based on Fig. 4, it is possible to describe the transfer function ω_m / T_L as eq. (11). Compared with the transfer function under the classical PI control, i.e., eq. (12), it can be found that eq. (11) is equal to eq. (12) multiplied by $s^2/(2ks+k^2-s^2)$, which has high-filter characteristics. Therefore, disturbance effects are more damped below the frequency $k(rad/s)$. Then, considering the transfer functions of ω_m / ζ, i.e., eq. (13-14), the influence of the measurement noise with the disturbance compensation is declined because of a low-pass filter factor $1-J_m(2ks+k^2)s/[K_T(s+k)^2(k_p s+k_i)]$. Therefore, the influence of the measurement noise can be reduced.

$$-\frac{\omega_m}{T_L}=\frac{s^2}{2ks+k^2-s^2}\frac{s}{J_m s^2+K_T(K_p s+K_i)} \tag{11}$$

$$-\frac{\omega_{m\text{-}PI}}{T_{L\text{-}PI}}=\frac{s}{J_m s^2+K_T(K_p s+K_i)} \tag{12}$$

$$-\frac{\omega_m}{\zeta}=\frac{K_T(K_p s+K_i)(s+k)^2-J_m(2ks+k^2)s}{[J_m s^2+K_T(K_p s+K_i)](s+k)^2} \tag{13}$$

$$=\frac{K_T(K_p s+K_i)}{J_m s^2+K_T(K_p s+K_i)}\left(1-\frac{J_m(2ks+k^2)s}{K_T(s+k)^2(K_p s+K_i)}\right)$$

$$-\frac{\omega_{m\_PI}}{\xi_{PI}}=\frac{K_T(K_p s+K_i)}{J_m s^2+K_T(K_p s+K_i)} \tag{14}$$

B. Feedback of the Estimated Speed Vibration

A large K_p may bring vibration to the operation portion, and this vibration is transmitted to the feedback of the speed loop. If the speed vibration signal is extracted, then it is possible to offset the vibration by adding it to the speed feedback.

A band-pass filter is appropriate to deal with certain frequency vibrations concerned with speed. Assuming ω_{lf}, ω_{hf} is the cut-off frequency of the low-pass filter and high-frequency filter, and the bandwidth of the band-pass filter is $\omega_{hf}-\omega_{lf}$. Fig. 5 shows the frequency response of the high-pass+low-pass filter, the band-pass filter, and the high-pass+band-pass filter, where $\omega_{lf}=628rad$ and $\omega_{hf}=1000\,rad$. This figure also illustrates that the high-pass+low-pass filter has the same characteristics as the band-pass filter. Furthermore, from the Fig. 3, it can be seen that the transfer function $\hat{\omega}_{err}(s)/\omega_m(s)$, is actually a high-pass filter, which is denoted by eq. (15). Therefore, it is only necessary to design an additional low-pass filter to extract the vibration signal. The estimation of the whole speed vibration is simple within this structure.

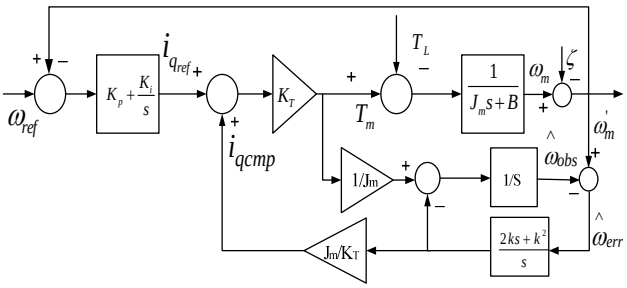

Fig. 4. The disturbance observer.

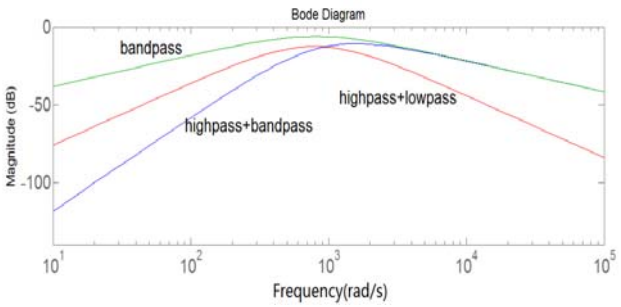

Fig. 5. Frequency response of three different types of filters.

$$\frac{\hat{\omega}_{err}}{\omega_m}=\frac{s}{s+k_{vib}} \tag{15}$$

C. Control Parameters Design

1) Online Spectrum Analysis: Since the proposed method needs to extract the vibration signal, the frequency of the vibration should be known. The DFT (discrete Fourier transform) is applied to analyze the speed error between the motor speed and the speed reference. When an ADC (analog-to-digital conversion) is applied to the motor speed error at an approximate sampling rate over the observation interval T=N*Ts, where N is the number of acquired samples and Ts is the sampling period, the finite discrete-time sequence of the speed error can be obtained:

$$Spderr\ (kT_s)=\sum_{n=0}^{N-1} Spderr\ (n)W_N^{kn}$$

$$W_N^{kn}=e^{-j2\pi/N} \qquad k=0,1\ldots N-1$$

$Spderr\ (kT_s)$ is the kth harmonics. In order to shorten the DFT calculation time in practice, the FFT is used. Actually, the FFT is widely used in control systems. Q. G.Wang and J. J. Nelson processed signals by using the FFT, and frequency spectra are added to the feedback signal [7], [8]. R. Blasco-Gimenez used the FFT to measure motor speed [9], and N. Baoliang suppressed the vibration magnitude by analyzing

the FFT spectrum of vibration signals [10]. The speed error acquisition uses the DMA with buffering for date collection and processing. Then the discrete date is transformed to the frequency domain according to the FFT algorithm. Thus, the power spectrum density can be calculated by squaring the amplitude of the FFT output. The vibration frequency ω_{vib} corresponds to the largest PSD.

In this paper, a STM32F302 is used as the control unit. Its powerful calculation ability makes the realization of the FFT analysis easy. It only takes about 1.3ms when N=1024. Therefore, it is suitable for the real time control of high dynamic PMSM servo systems. In the experiments, N=1024 is adopted.

2) The Design of the Disturbance Observer Parameters k: According to the discussion about the disturbance observer design in the previous section, we can see that a large k is helpful for interference rejection, while a small *k* can improve the measurement noise rejection. As the system cut-off frequency under PI control is near $\sqrt{K_T K_p/(\tau J_m)}$, we recommend that k be no bigger than $\sqrt{K_T K_p/(\tau J_m)}$, considering the reliability of both.

3) The Design of the Vibration Suppression Parameters k_{vib} and k_{lf}: After finding the vibration frequency using the FFT, it is possible to define $k_{vib}=\omega_{vib}$ in order to extract the vibration signal and to simplify the calculation of the design processes. Then the design of k_{lf} is analyzed. Firstly, the transfer function between ω_{ref} and ω_m is considered with the speed vibration compensation ω_{cmp} as follows (T_f=0 and B=0 are assumed for the sake of simplicity) :

$$G_2 = K_T(K_p + \frac{K_i}{s})\frac{1}{J_m s} \tag{16a}$$

$$H_2 = 1 + \frac{s}{s+\omega_{vib}}\frac{k_{lf}}{s+k_{lf}} \tag{16b}$$

$$G_{rm}(s) = \frac{\omega_m(s)}{\omega_{ref}(s)} = \frac{G_2}{1+G_2H_2} \tag{16c}$$

The characteristic polynomial in the closed loop from the above equations can be written as:

$$\Delta P(s) = 1 + G_2H_2 = a_4s^4 + a_3s^3 + a_2s^2 + a_1s + a_0$$

$$a_4 = J_m$$

$$a_3 = J_m(\omega_{vib} + k_{lf}) + K_TK_p$$

$$a_2 = K_iK_T + K_TK_p(\omega_{vib} + 2k_{lf}) + J_m\omega_{vib}k_{lf}$$

$$a_1 = K_TK_p\omega_{vib}k_{lf} + K_iK_T(\omega_{vib} + 2k_{lf})$$

$$a_0 = K_iK_T\omega_{vib}k_{lf}$$

and the numerator polynomial is:

$$\Delta N(s) = K_pK_Ts^3 + [K_pK_T(\omega_{vib}+K_{lf}) + K_iK_T]s^2 + [K_pK_T\omega_{vib}k_{lf} + K_iK_T(\omega_{vib}+k_{lf})]s + K_iK_T\omega_{vib}k_{lf}$$

In order to offset the peak of eq. (16c) at the resonance frequency, $|G_{rm}(s)|$=1 is expected at the resonance frequency. Then the following equations can be obtained:

$$\left|\frac{jb_1+b_0}{ja_1+a_0}\right| = 1$$

$$a_1 = [-(J_m(k_{lf}+\omega_{vib}) + K_pK_T)\omega_{vib}^2 + K_TK_p\omega_{vib}k_{lf} + K_TK_i(\omega_{vib}+2k_{lf})]\omega_{vib}$$

$$a_0 = K_TK_i\omega_{vib}k_{lf} - (J_m\omega_{vib}k_{lf} + K_TK_i + K_pK_T(\omega_{vib}+2k_{lf}))\omega_{vib}^2$$

$$b_1 = [-K_pK_T\omega_{vib}^2 + K_TK_p\omega_{vib}k_{lf} + K_TK_i(\omega_{vib}+k_{lf})]\omega_{vib}$$

$$b_0 = K_TK_i\omega_{vib}k_{lf} - [K_TK_i + K_pK_T(\omega_{vib}+k_{lf})]\omega_{vib}^2$$

Since it is known that ω_{vib} is close to $\sqrt{K_TK_p/(\tau J_m)}$ as discussed in section II.C, it can be supposed that $\tau J_m\omega_{vib}^2 \approx K_TK_p$. In addition, since K_i is equal to K_p/τ, it is possible to further simplify a_1, a_0, b_1, b_0. Assuming that $k_{lf} = m\omega_{vib}$, it is possible to obtain the following equations:

$$a_1 = K_TK_p\frac{m+1}{2}$$

$$a_0 = -K_TK_p\frac{m+1}{2}$$

$$b_1 = K_TK_p(m-\frac{3}{2})$$

$$b_0 = -K_TK_p\frac{3}{2}$$

$$\frac{(\frac{1}{2}(m+1))^2 + (-\frac{1}{2}(m+1))^2}{(m-\frac{3}{2})^2 + (\frac{3}{2})^2} = 1 \tag{17}$$

From eq. (17), there are two solutions, $m = 6.8$ and $m = 1.17$. However, in order to guarantee the phase margin at the resonance frequency, $a_1 > 0$ should be satisfied as $b_1 > 0, b_0 < 0, a_0 < 0$. As a result, only $m = 6.8$ can be the solution. Therefore:

$$k_{lf} = 6.8\omega_{vib} \tag{18}$$

4) The Proof of the Vibration Suppression by Using the Proposed Method: So far, all the control parameters have been designed. Now the merits of the proposed method can be analyzed by comparing the speed command response and disturbance resistance under the proposed method and the classical PI control.

The simulation parameters in Table I are used to test the characteristics of both transfer functions. Firstly, the PI control structure in Fig. 1 is built under the Simulink environment. The speed error data is transfered to the frequency domain by the FFT algorithm. The frequency spectrum of ω_{err} when K_p=3.45 is shown in Fig. 6(a). From this picture, it can be seen

that the vibration frequency is $\omega_{vib} = 392.5 rad/s$, which is close to $\sqrt{K_T K_p / (\tau J_m)} \approx 464\ rad/s$. Based on $\omega_{vib} = 392.5 rad/s$ and eq. (18), it is possible to calculate $k_{vib} = 392.5 rad/s$ $k_{lf} = 2669\ rad/s$. Then bode diagrams of the disturbance response and speed command response can be plotted under the proposed method and the classical PI control. The results are shown in Fig. 6(b) and 6(c). From Fig. 6(b), it can be seen that the low-frequency magnitude of the disturbance response is much more dampened with the proposed method than with the PI control. In addition, the resonance peak of the disturbance response at the resonance frequency is canceled by the proposed method. Similarly, Fig. 6c compares the speed command responses under the two control methods. It is obvious that the magnitude of the classical PI controller is higher than that of the proposed method at the resonance frequency. Actually, the magnitude is near 0dB under the proposed method which is what is expected according to the design in section III.C. In conclusion, the proposed method has better speed command and disturbance rejection performance than the PI control. Therefore, the concept of reducing the resonance peak to suppress vibrations can be achieved by the proposed method.

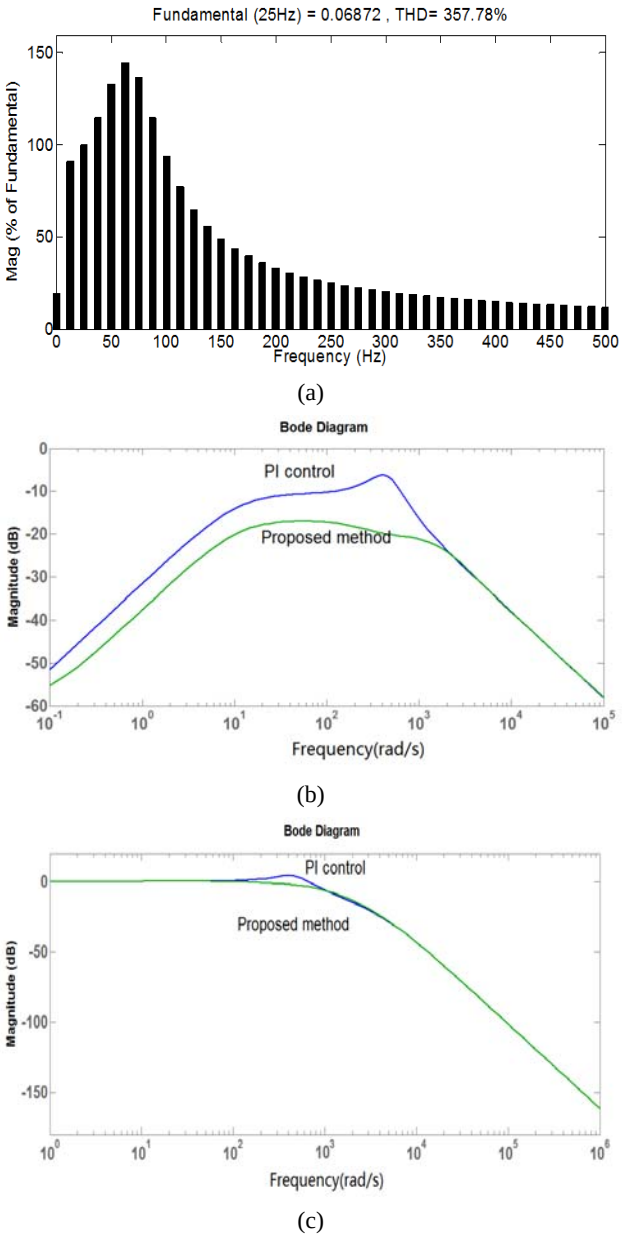

Fig. 6. (a) The frequency spectrum of the speed error. (b) The bode of disturbance response. (c) The bode of speed command response.

IV. Simulation and Experimental Results

A. Simulation Results

In this section, the classical PI control and the proposed control method are compared. The simulation parameters are the same as those in Table I. Fig. 7(a)-(e) show the motor speed response and current response with different values of K_p under the PI control and the proposed method. In Fig. 7(a), it can be seen that the speed overshoot under the PI control is 20% compared with 16% under the proposed method. It can also be seen in Fig. 7(b)-(c) that vibrations and a larger overshoot occur when K_p increases under the PI controller, while the current and speed response using the proposed method has a shorter settling time and a smaller overshoot. In Fig. 7(d)-(e), it can be seen that K_p is too large. As a result, the speed and current vibrations last for a long time under the PI control. Meanwhile the system is still stable under the proposed method. Fig. 7(f) shows the frequency spectrum of the speed error under the proposed method. Compared with Fig. 6(a), the content of the vibration frequency is significantly decreased. Since disturbance rejection is also an important performance index, the disturbance response is also tested. A step disturbance torque $T_L = 1 N.m$ is input at $t = 0 s$. The results are shown in Fig. 8, and it can be seen that the speed loss under the proposed method is smaller than that under the PI control, and the recovery time is also smaller.

B. Experimental Results

To show that the proposed method is valid in practice, a general diagram of the proposed control is declared as in Fig. 9(a). An experimental platform is set up as in Fig. 9(b). The platform consisted of a PMSM, a servo driver, and a PC for recording the results. The PMSM is a 80MSL02430 made by Maxsine Company, China. The motor parameters are J_m=3.5*10e-4 and I_N=4.4A. Both the PI control system and the proposed control system are tested for comparison.

The speed step response ($n = 100\ r/\min$) results are shown in Fig. 10-12. The K_p unit is Hz, and it is the inside unit in the DSP. Fig. 10-11 describe the speed response with different values of K_p. At the same time the corresponding show the motor speed results when the disturbance torque is added suddenly under the two control methods. From Fig.

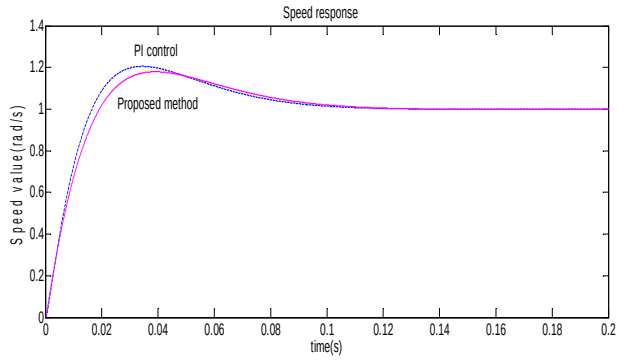

(a)

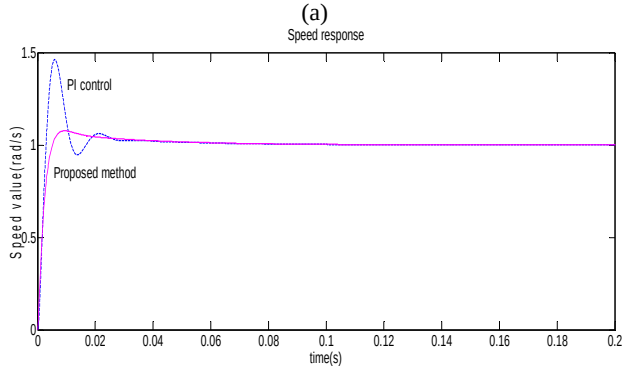

(b)

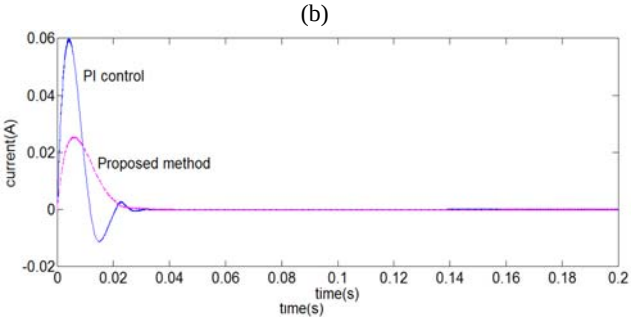

(c)

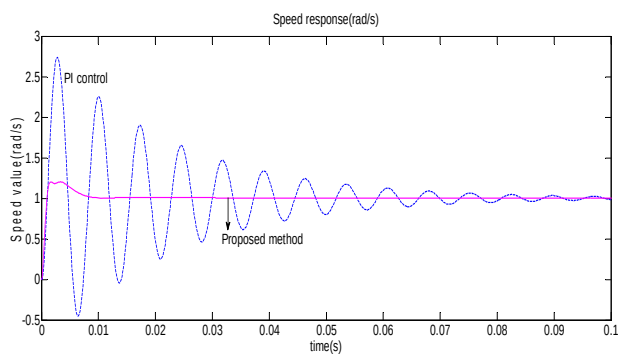

(d)

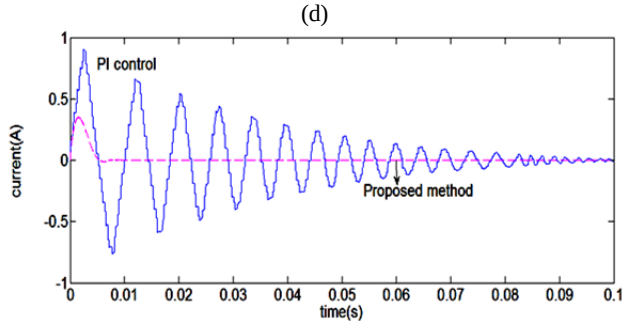

(e)

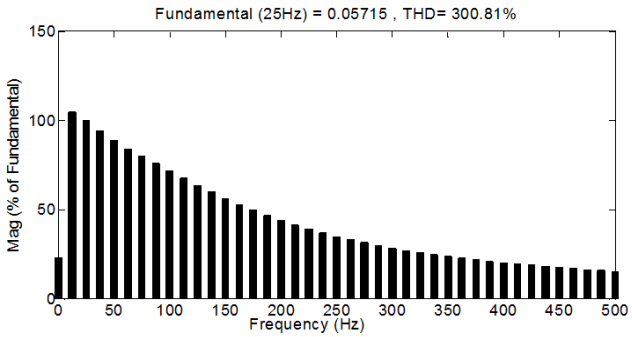

(f)

Fig. 7. (a) The motor speed response under different K_p=0.69. (b) The motor speed response with Kp=3.45. (c). Current response with Kp=3.45. (d). The motor speed response under different Kp=20.7 (e). Current response with Kp=20.7. (f). The Speed error frequency spectrum under the proposed method.

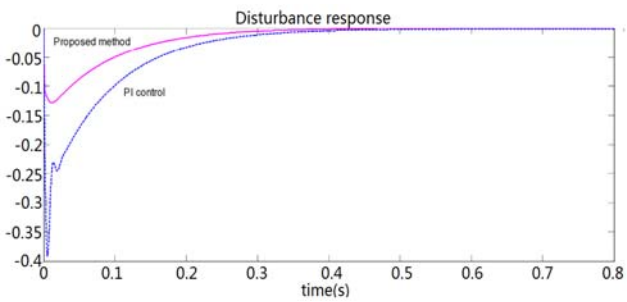

Fig. 8. The disturbance response of the motor speed under the PI control and proposed method.

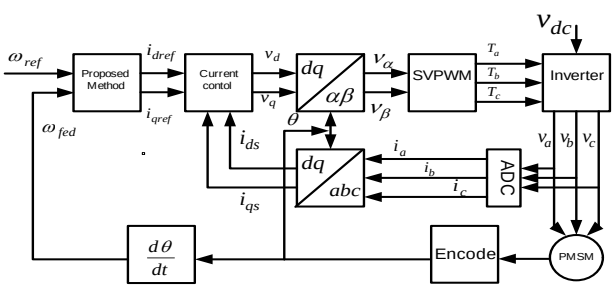

(a)

(b)

Fig. 9. (a) Software structure and experimental platform. (b) Experimental platform.

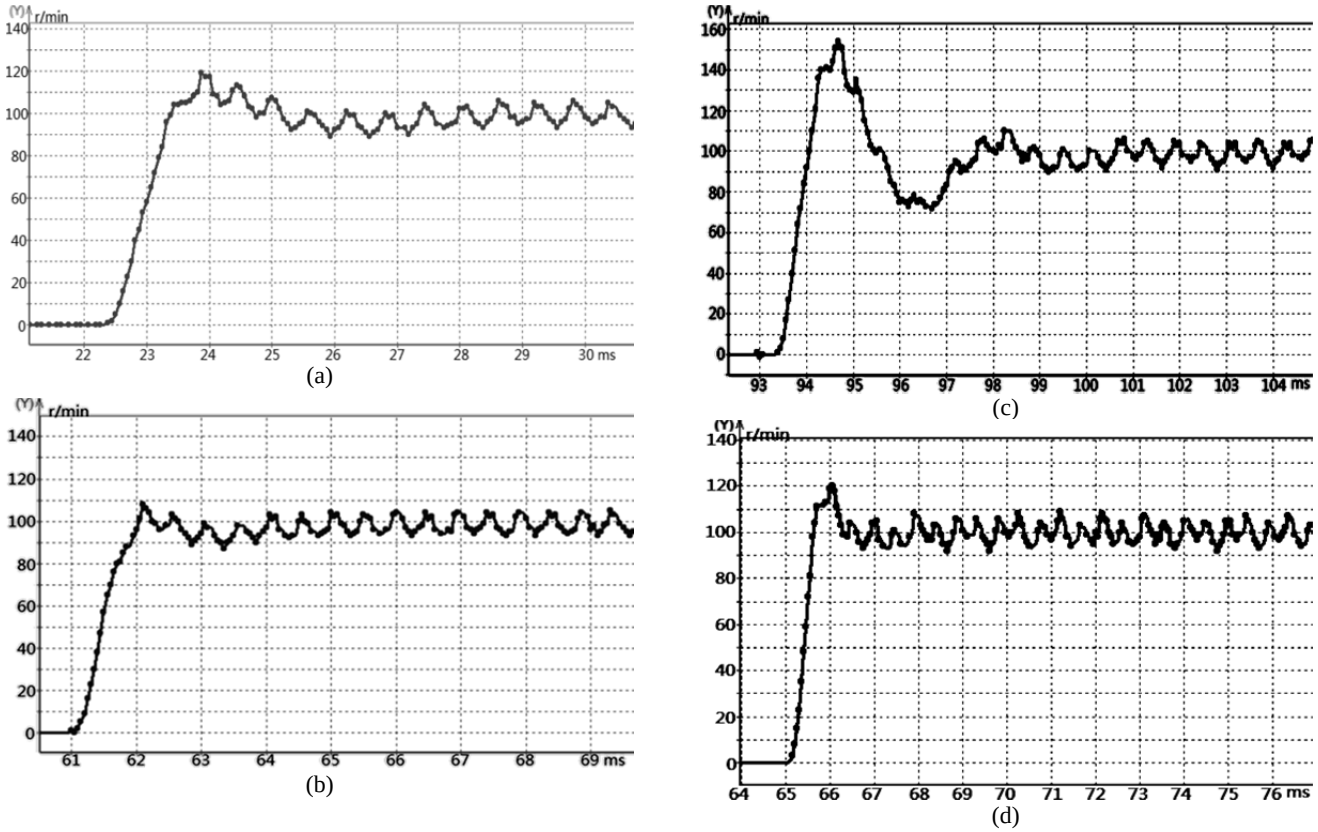

Fig. 10. (a) Speed step response with Kp=174Hz under PI control. (b) Speed step response with Kp=174Hz under proposed method. (c) Speed step response with K_p=*260Hz* under PI control. (d) Speed step response under the proposed method Kp=260Hz.

TABLE II
COMPARISON UNDER PI CONTROL AND PROPOSED METHOD

items	overshoot		Vibration	
	PI	Propo	PI	Propos
Kp=170	20%	10%	4ms	2ms
Kp=260	55%	20%	7ms	2ms
Kp=420	uncontro	40%	>15ms	4.5ms

current signals are also shown in Fig. 12(a)-(d). The current responses and the speed responses coincided. Table II shows a comparison of the speed response between the PI control and the proposed method.

From Table II it can be seen that the performance of the PI controller becomes worse as Kp increases, while the proposed method still has good features when Kp is high. Compared with the simulation results, the same trends are seen. The overshoot of the speed responses with the proposed method is reduced by two times compared with the corresponding results of the PI controller in the simulation and experiments. In Fig. 11(a) and Fig. 12(c), it can be seen that the speed and current responses vibrates for a long time just like those in the simulation in Fig. 7(d)-(e). However, by using the proposed method, the vibration time is reduced remarkably. The simulation results in Fig. 7(d) vibrated for 1-2 periods under the proposed method which is basically same as the experimental results in Fig. 11(b). Additionally, Fig. 13(a)-(b)

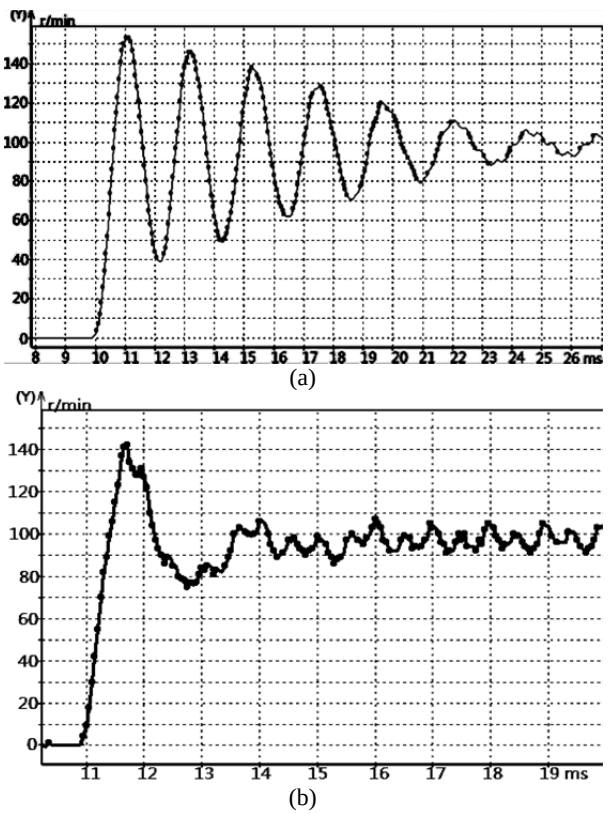

Fig. 11. (a) Speed step response with Kp=420Hz under the PI control. (b) Speed step response with Kp=420Hz under the proposed method.

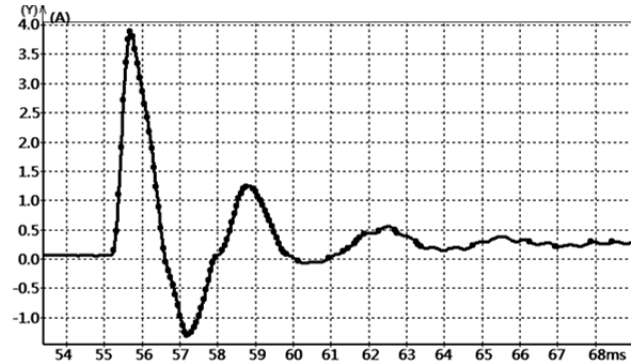

(a)

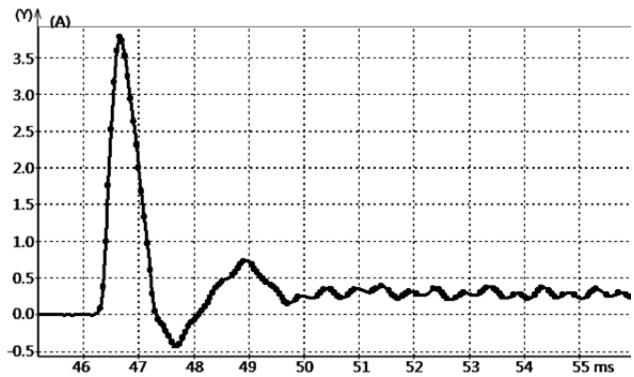

(b)

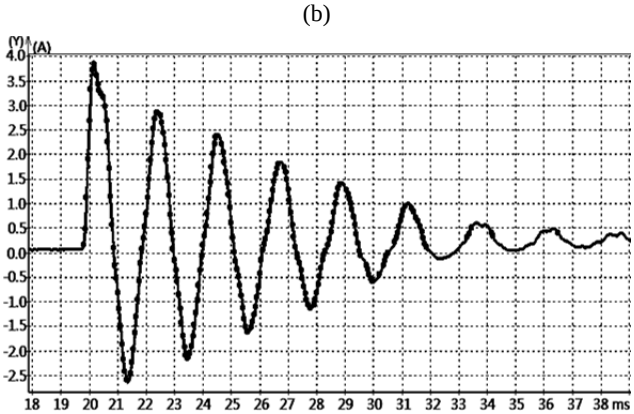

(c)

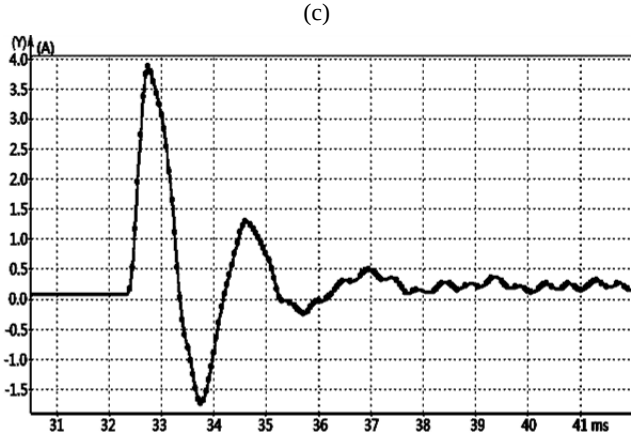

(d)

Fig. 12. (a) Current response with Kp=260Hz under PI control. (b) Current response under proposed method Kp=260Hz. (c) Current response with Kp=420Hz under PI control. (d) Current response under proposed control Kp=420Hz.

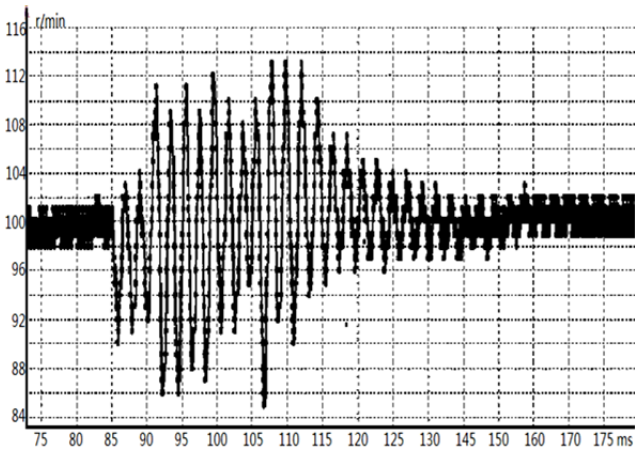

(a)

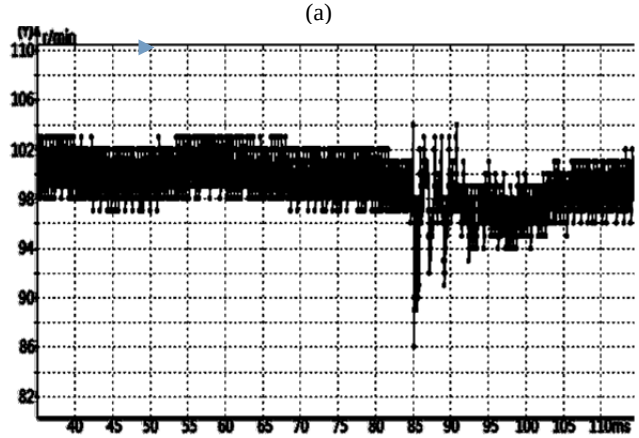

(b)

Fig. 13. (a) Disturbance results with Kp=420Hz under the PI control. (b) Disturbance results with Kp=420Hz under proposed method.

13(a), it can be seen that speed vibrations happen because of disturbances. In addition, the vibration frequency is the same as the speed step response in Fig. 11(a). However, under the proposed method, the vibration is suppressed in Fig. 13b. This is also consistent with the bode diagram of the transfer function between the disturbance in the motor speed in Fig. 6b. Actually, the load disturbance may cause speed vibrations. However, this does not change the resonance frequency if Kp is invariable. The analysis in section II.C also shows the relative parameters which affects the oscillation frequency. Therefore, if the speed oscillation frequency is detected accurately, the proposed method is effective even if the load disturbance is variable. To verify this, a variable disturbance torque based on the previous disturbance experiment was added. Fig. 14 shows the speed response result. It can be see that although the speed has some fluctuations, the resonance induced by the high Kp is suppressed. In conclusion, through the experimental results, it can be seen that the corresponding characteristics of the PI control and the proposed method are consistent with the simulation performance. It can also be seen that the proposed method is efficient in terms of vibration suppression which is induced by improving the Kp. It also performs well under disturbances.

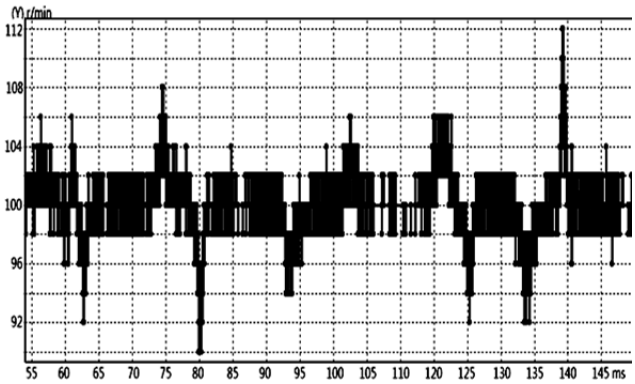

Fig. 14. The speed response with Kp=420Hz and variable disturbance.

V. CONCLUSION

In this paper, the essential reasons for vibrations with a high speed-loop gain are described. Then the vibration suppression method is presented. The basic idea of the method is to counteract the resonance peak at the resonance frequency. An online spectrum analysis FFT was utilized to detect the vibration frequency ω_{vib}. Then the vibration signal was extracted as the compensation for the speed feedback by using a low-order speed observer and a low-pass filter. The disturbance observer is a low-order Luenberger observer, which helps improve the anti-disturbance ability. Additionally, the design of the controller parameters is an important key to implementing the proposed method in practice. Design processes that are too complex are tough for realization. In this paper, simply design rules were obtained by analyzing the system transfer functions. The parameter k is relative to $\sqrt{K_T K_p /(\tau J_m)}$ and $k_{lf} = 6.8\omega_{vib}$. Bode diagrams of the frequency response under the classical PI controller and the proposed method illustrate the vibration suppression principle in theory and show that the resonance peak can be successfully reduced by the proposed method. The experimental results also show that the proposed method can effectively suppress vibration in a PMSM servo driver. The overshoot is smaller and the settling time is reduced.

REFERENCES

[1] R. Wang, "Study on AC servo driven system and it"s novel control strategy," College of Electrical Engineering, Zhejiang University, 2005.

[2] C. Ma., J. Cao, and Y. Qiao, "Polynomial- method-based design of low-order controllers for two-mass systems," *IEEE Trans. Ind. Electron.*, Vol. 60, No. 3, pp. 969-978, Mar. 2013.

[3] C. Ma and H. Y. Backlash, "Vibration suppression in torsional system based on the fractional order- Q-filter of disturbance observer," in *Proc 8th IEEE Int. Workshop Adv. Motion contr*., pp. 577-582, 2004.

[4] C. Ma and Y. Hori., "The application backlash of fractional order control to vibration suppression," in *Proc Conf. American Contr*, Vol. 3, pp. 2901-2906, 2004.

[5] W. Li and Y. Hori, "Vibration suppression using single neuron-based PI fuzzy controller and fractional-order disturbance observer," *IEEE Trans. Ind. Electron.*, Vol. 54, No. 1, pp. 1117-126, Feb. 2007.

[6] J.-K. Seok, D.-H. Kim, and D.-C. Lee, "Automatic Mode Switching of P/PI Speed Control for industry servo drives using online spectrum analysis of torque command," *IEEE Trans. Ind. Electron.*, Vol. 54, No. 5, pp. 2642-2647, Oct. 2007.

[7] Q.-G.Wang, Q. Bi, and B. Zou, "Use of FFT in delay feedback systems," *Electon. Lett.*, Vol. 33, No. 12, pp. 1099-1100, 1996.

[8] J. J. Nelson, G. Venkataramanan, and A. M. El-Refaie, "Fast thermal profiling of power semiconductor devices using Fourier techniques," *IEEE Trans. Ind. Electron.*, Vol. 53, No. 2, pp. 521-529, Apr. 2006.

[9] R. Blasco-Gimenez, G. M. Asher, M. Summer, and K. J. Bradley, "Performance of FFT rotor slot harmonic speed detector for sensorless induction motor drives," in *Proc. IEE-Elect. Power Appl*, Vol. 143, No. 3, pp, 258-268, 1996.

[10] N. Baoliang and Y. Xia, "A FFT-based variety sampling-rate sine sweep vibration controller," in *Proc. Neural Netw. and Signal Process. Conf*, Vol. 2, pp, 1714-1718, 2003.

[11] S. Manabe, "Sufficient condition for stability and instability by Lipatov and its application to be coefficient diagram method," *9th Workshop on Astro-dynamics and Flight Mechanics, ISAS*, 1999.

[12] S. Manabe, "The coefficient diagram method," *14th IFAC Symposium on Automatic control in Aerospace*, 1998.

[13] J.-S. Ko, Y.-G. Seo, and H.-S. Kim, "Precision position control of PMSM using neural observer and parameter compensator," *Journal of Power Electronics*, Vol. 8, No. 4, pp. 354-362, Oct. 2008.

[14] W.-C. Wang, T.-H. Liu, and K.-Y. Fan, "Design and implementation of a wavelet speed controller with application to micro- permanent magnet synchronous motor drives," *IET Electric Power Applications*, Vol. 7, No. 4, pp. 245-255, Apr. 2013.

[15] S. Manabe, "Application of coefficient diagram method to MIMO system," *10th Workshop on Astrodynamics and Flight Mechanics, ISAS*, 2000.

[16] A. Bahr and S. Beineke, "Mechanical resonance damping in an industrial servo drive," *IEEE European Conf, Power Elec. and Appl*, pp. 1-10, 2007.

[17] Z. Zhiqiang, H. Yuqing, Q. Juntong, H. Jianda, and W. Tianran, "The analysis and synthesis of PID controller based on closed loop response characteristics," in *Proc. Robotics and Biomimetics (ROBIO), 2012 IEEE International Conference on*, pp, 1930-1936, 2012.

[18] M. Hanifzadegan and R. Nagamune, "Tracking and structural vibration control of flexible ball–screw drives with dynamic variations," *IEEE/ASME Trans. Mechatron.*, Vol. 20, No. 1, pp. 133-141, Feb. 2015.

[19] K. Szabat, T. Tran-Van, and M. Kaminski, "A modified fuzzy luenberger observer for a two-mass drive system," *IEEE Trans. Ind. Inform.*, Vol. 11, No. 2, pp. 531-539, Apr. 2015.

[20] S. E. Saarakkala and M. Hinkkanen, "State-space speed control of two-mass mechanical systems, analytical tuning and experimental evaluation," *IEEE Trans. Ind. Appl.*, Vol. 50, No. 5, pp.3428-3437, Sep./Oct. 2014.

[21] R. Musznski and J. Deskur, "Damping of torsional

vibration in high-dynamic industrial drives," *IEEE Trans. Ind. Electron.*, Vol. 57, No. 2, pp. 554-552, Feb. 2010.
[22] I. U. Khan and R. Dhaouadi, "Robust control of elastic drives through immersion and invariance," *IEEE Trans. Ind. Electron.*, Vol. 62, No. 3, pp. 1572-1580, Oct. 2014.
[23] D. Heng, H. Wang, and K.-Y. Huang, "Design of PMSM driver system digital PI adjuster parameters," *Electric Drive*, Vol. 39, No. 1, pp. 7-9, 2009.

Qiong Li was born in China, in 1989. She received her B.S. degree in Electrical Engineering from East China Jiaotong University, Jiangxi, China. She is presently working towards her Ph.D degree in Electrical Engineering at the Huazhong University of Science and Technology, Wuhan, China. Her current research interests include high-performance servo drivers and the control of robots in industrial fields.

Qiang Xu was born in China, in 1968. He received his B.S., M.S., and Ph.D. degrees in Electrical Engineering from the Huazhong University of Science and Technology, Wuhan, China. He is presently working as a professor in the Department of Electrical Engineering, Huazhong University of Science and Technology. His current research interests include high-performance servo drivers and the control of robots in industrial fields.

Shenghua Huang was born in China, He is presently working as a professor in the Department of Electrical Engineering, Huazhong University of Science and Technology. His current research interests include high-performance servo drivers .